



The University of
Nottingham

UNITED KINGDOM • CHINA • MALAYSIA

Zeng, Xuesen and Brown, Louise P. and Endruweit, Andreas and Long, Andrew C. (2012) Advanced geometry modelling of 3D woven reinforcements in polymer composites: processing and performance analysis. In: Fourth World Conference on 3D Fabrics and their Applications, 10-11 Sep 2012, Aachen, Germany.

Access from the University of Nottingham repository:

http://eprints.nottingham.ac.uk/2052/1/Endruweit%2C_Andreas_-_Advanced_geometry_modelling_of_3D_woven_reinforcements.pdf

Copyright and reuse:

The Nottingham ePrints service makes this work by researchers of the University of Nottingham available open access under the following conditions.

This article is made available under the University of Nottingham End User licence and may be reused according to the conditions of the licence. For more details see:
http://eprints.nottingham.ac.uk/end_user_agreement.pdf

A note on versions:

The version presented here may differ from the published version or from the version of record. If you wish to cite this item you are advised to consult the publisher's version. Please see the repository url above for details on accessing the published version and note that access may require a subscription.

For more information, please contact eprints@nottingham.ac.uk

Advanced Geometry Modelling of 3D Woven Reinforcements in Polymer Composites: Processing and Performance Analysis

Xuesen Zeng^{*}, Louise P. Brown, Andreas Endruweit, Andrew C. Long
Faculty of Engineering – Division of Materials, Mechanics & Structures,
University of Nottingham, University Park, Nottingham, NG7 2RD, U.K.

^{*}Corresponding Author. Email: xuesen.zeng@nottingham.ac.uk

ABSTRACT

Numerical methods have become increasingly effective tools for analysis and design of composite materials. This study investigates how the inclusion of geometrical variations in modelling 3D woven fabrics affects the accuracy of numerical predictions. Based on micro-Computed Tomography data of 3D orthogonal woven composites, unit cell models were generated in TexGen at different levels of geometrical detail. Two types of analysis were implemented: (a) computational fluid dynamics (CFD) simulates resin flow during fabric impregnation in composites processing to predict permeability; (b) implicit static finite element analysis predicts in-plane tensile strength of the composites. By comparison with experimental data, the numerical predictions indicate that local geometrical variations, particularly in yarn cross-section, surface crimp and binder yarn path, have significant influence on both permeability and material strength. It is important to model the precise geometry in certain locations while the overall geometry can be simplified in order to maintain the practicality of model generation.

Keywords: textile composite, orthogonal weave, numerical modelling, permeability, mechanical analysis

1. Introduction

One of the major challenges in modelling composite materials, especially those with 3D woven reinforcement, is the complex hierarchical internal structure of textiles and its variation due to local deformations. The microstructure of 3D woven composites dictates many material properties. While impact strength and damage tolerance are improved compared to 2D weaves, the introduction of through-thickness binders in 3D fabrics has mostly detrimental effect on in-plane properties including stiffness, strength and fatigue strength, according to a recent review of published experimental data [1]. The microstructure of the reinforcement also determines flow of the penetrating matrix resin during composite manufacture, which has a strong influence on the quality of the finished component, in particular regarding defect formation. To advance the utilisation of 3D woven fabrics for industrial applications, it is crucial to understand and quantify the microstructure and its effect on processing parameters and mechanical properties.

2. Geometrical characterisation

As an example, a carbon fibre orthogonal weave with the specifications listed in Table 1 was characterised in this study. The internal geometry of composites with the orthogonal weave as reinforcement was characterised thoroughly at different compaction levels by micro-Computed Tomography (μ -CT) analysis. The geometrical parameters extracted from the analysis are assumed to be applicable for generating predictive geometrical models of similar composites without the need for detailed measurement. The 3D image data can be analysed conventionally by taking measurements manually slice by slice. Alternatively, to avoid intensive labour, automated image processing and measurement has been implemented with the help of MatLab® Image Toolbox.

Table 1. Specifications of 3D reinforcement characterised here.

| Fabric style | Orthogonal weave |
|------------------------------------|------------------|
| Areal density (kg/m ²) | 4.775 |
| Number of warp layers | 6 |
| Warp yarn | 12K |
| Warp yarn linear density (g/km) | 800 |
| Number of weft layers | 7 |
| Weft yarn | 6K × 2 |
| Weft yarn linear density (g/km) | 800 |
| Binder yarn | 1K |
| Binder yarn linear density (g/km) | 67 |

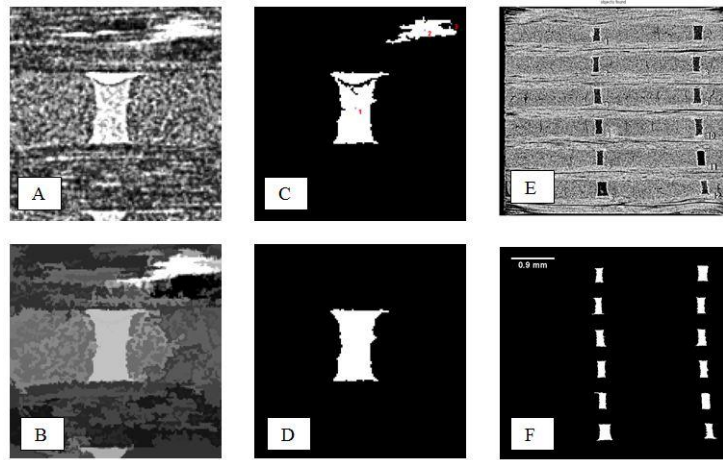


Figure 1. Image segmentation of flow channel in 3D carbon fibre reinforcement. A-D: progressive image operations to isolate flow channel region; E: labelled flow channels in original μ -CT image; F: binary image of flow channels.

The measurements include geometrical parameters such as the area (A_c), the centroid (X) and the height (h) of flow channels in a cross-section. The yarn spacing (l) is the distance between the centroids of two neighbouring channels ($\|X_i - X_{i-1}\|$). Given the filament radius (r) and the number of filaments (N) in each yarn, the fibre volume fraction of each yarn cross-section can be calculated according to Equation (1).

$$V_f = \frac{A_{\text{total fibre}}}{A_{\text{yarn}}} = \frac{N\pi r^2}{hl - A_c} \quad (1)$$

To measure flow channels in weft and warp directions, the 3D images are re-sliced and analysed in each direction. Summary data for composites with two different fibre volume fractions are listed in Table 2.

Table 2. Geometry measurements for the orthogonal reinforcement at different compression levels.

| | Number of measurements | Yarn width (mm) | Yarn height (mm) | n in power ellipse (Eq. 3) | Yarn gap (mm) |
|--------------------------------|------------------------|---------------------------|----------------------------|----------------------------|----------------------------|
| $h = 5\text{mm}, V_f = 0.55$ | | | | | |
| Warp | 10755 | 1.88 ± 0.04 (2 %) | 0.41 ± 0.046 (11 %) | 0 | 0.33 ± 0.046 (14 %) |
| Surface layer weft | 39 | 2.13 ± 0.06 (3 %) | 0.39 ± 0.03 (8 %) | 1.4 / 0 | 0.32 ± 0.07 (22 %) |
| Internal layer weft | 4299 | 2.09 ± 0.08 (4 %) | 0.35 ± 0.06 (16 %) | 0.1 | 0.28 ± 0.06 (16 %) |
| Surface section binder | 4 | 0.62 ± 0.05 (9 %) | 0.15 ± 0.02 (10 %) | 1 | |
| Internal section binder | 119 | 0.34 ± 0.05 (15 %) | 0.21 ± 0.03 (13 %) | 0 | |
| $h = 4.1\text{mm}, V_f = 0.67$ | | | | | |
| Warp | 7319 | 1.90 ± 0.02 (1%) | 0.33 ± 0.02 (7%) | 0 | 0.14 ± 0.02 (17 %) |
| Surface layer weft | 23 | 2.32 ± 0.1 (4 %) | 0.29 ± 0.2 (8 %) | 1.2 / 0.5 | 0.08 ± 0.02 (25 %) |
| Inner layer weft | 5264 | 2.24 ± 0.06 (3 %) | 0.27 ± 0.02 (6 %) | 0 | 0.16 ± 0.04 (25 %) |
| Surface section binder | 6 | 0.89 ± 0.06 (7 %) | 0.07 ± 0.007 (10 %) | 0 | |
| Internal section binder | 116 | 0.25 ± 0.02 (8 %) | 0.23 ± 0.03 (12 %) | 0 | |

3. Geometrical modelling

In order to simplify and automate the generation of 3D textile models based on geometrical parameters, a 3D wizard has been implemented in TexGen [2], the textile geometry modelling software developed at Nottingham University. Weave pattern generation is customised for orthogonal, angle interlock, offset angle interlock and layer-to-layer weaves. A series of dialogs allow number of warp and weft yarns to be entered, as well as the number of layers of each and the ratio of binder to warp yarns. The width, height, spacing and cross-sectional shape can be specified for each set of yarns. The yarn cross-sections are approximated by power ellipses (Eqs. 2 and 3), which are generalized ellipses where the y coordinate is assigned a power n to make the section resemble a rectangle with rounded edges when $n < 1$ or a shape similar to a lenticular cross-section when $n > 1$. They are special cases of superellipse described by Gabriel Lamé [3].

$$C(v)_x = \frac{w}{2} \cos(2\pi v) \quad 0 \leq v \leq 1 \quad (2)$$

$$C(v)_y = \begin{cases} \frac{h}{2} \sin^n(2\pi v) & \text{if } 0 \leq v < 0.5 \\ -\frac{h}{2} (-\sin(2\pi v))^n & \text{if } 0.5 \leq v \leq 1 \end{cases} \quad (3)$$

Where w is yarn width and h is yarn height.

The subsequent weave pattern dialog allows for simple specification of the required weave pattern. In the case of the orthogonal weave, clicking on the binder/weft intersections toggles the binder between the top and bottom position on the textile as shown in Figure 2. The weave wizard then automatically generates the weave pattern, generating nodes on the yarn paths at each crossover point between warp/binder and weft yarns. Extra nodes are then positioned along the binder yarns to follow the contour of the outer weft yarns. At this stage, the geometry created is idealised with all yarns having constant cross sections.

With no refinement yet applied, there are intersections between the warp and weft yarns and the through thickness binder yarns. On examination of the μ -CT images it is also apparent that, even in the uncompacted fabric, the cross-sections of the outer weft yarns differ from those in the middle of the fabric. A refine option has, therefore, been implemented for the case of orthogonal weaves in order to model the geometry more realistically both in their uncompacted and compacted states. Throughout the process the volume fraction of the yarns are monitored so that they are maintained within realistic limits. To facilitate this, yarn properties are required as input for the warp, weft and binder yarns.

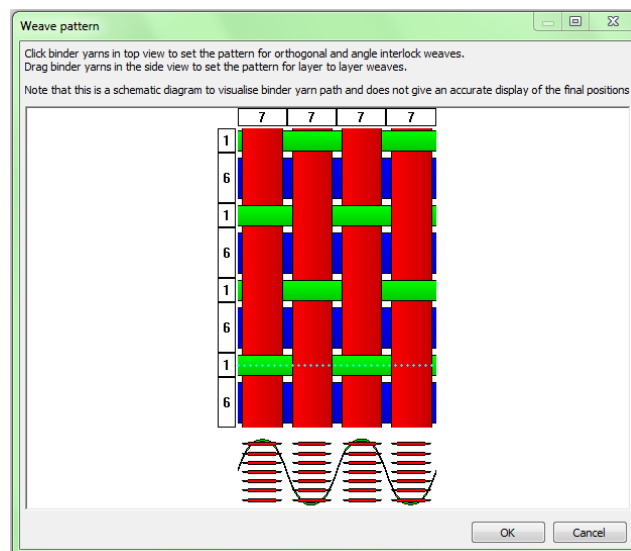


Figure 2. TexGen 3D Wizard: Orthogonal weave pattern dialog.

Firstly the cross-sections of the through thickness binder yarns are changed, if necessary, to fit into the available through thickness spaces between warp and weft yarns.

Next the heights of the warp and weft middle layers are adapted to model compaction on mould closure. An initial check of the space available will show whether it is possible to achieve a volume fraction for the yarn below the maximum specified. If not then TexGen will flag an error stating that the thickness requested cannot be achieved without exceeding the maximum volume fraction. It has been observed that the height of these yarns reduces in proportion to the total initial thickness of warp and weft layers. The height of the yarns is reduced accordingly and then the width increased so as to maintain the original volume fraction. If this cannot be achieved then the power of the power ellipse section used is increased, thus increasing the area, potentially to a rectangular section filling the space available.

The cross-sections of the outer weft yarns are then changed to give a section which more accurately represents the real textile, at the same time reducing the height to reflect the requested compaction. Where necessary the height is reduced further to allow for the, similarly reduced, thickness of the binder yarn which is incorporated into the height available for the weft yarn.

Finally the outer binder yarn cross-sections are changed to give a section which is flat on the outer surface. The widths of the binder yarns are increased as necessary to maintain the volume fraction. If the required height cannot be achieved then, if possible, the height of the weft yarn is reduced further. Failing this, crimp is introduced into the weft yarn to achieve the overall textile thickness and the cross-section of the warp yarn below is adjusted to remove resultant intersections in the yarns.

Figure 3a shows the orthogonal weave with the refine option selected but no change to the initial fabric thickness of 6.315 mm. The refinement here is limited to the binder yarns, which are adjusted through thickness, and the outer weft yarns. Figures 3b and 3c show the fabric compacted to thicknesses of 5.03 mm and 4.432 mm. Figure 3c shows the addition of a small amount of crimp in the outer weft yarn, necessary to achieve this degree of compaction. Comparison with the μ -CT images shows that, based on the assumptions mentioned above, TexGen is capable of modelling the geometry realistically down to a fabric thickness of 5.03 mm ($V_f = 55\%$). At a higher compaction level (thickness 4.432 mm), deviations between the TexGen model and the real geometry occur, noticeably in surface yarn cross-sections. Manual modification is required in this case.



Figure 3. Orthogonal weave generated using 3DWizard refine option. (a) original fabric thickness, 6.315 mm; (b) fabric thickness 5.03 mm; (c) fabric thickness 4.432 mm.

4. Flow modelling

To determine the textile permeability, which affects impregnating resin flow in composites processing, flow through the textile unit cell was simulated using Computational Fluid Dynamics (CFD) software. The yarns in the unit cell were modelled as porous media. The yarn permeability as input parameter was calculated using Gebart's analytical model [4]. At the interfaces between the porous yarns and the inter-yarn flow channels, conservation of fluid mass and momentum was assumed. Periodic boundary conditions were set on opposite faces of the textile unit cell both in weft and warp directions. Non-slip walls are specified for top and bottom faces to simulate the boundary conditions during the in-plane permeability test [5]. A pressure drop is applied on opposite faces of the unit cell. Dry air at 25 °C under atmospheric pressure was selected as fluid for simulation of steady state laminar flow through the fabric. A voxel mesh was chosen for the current study as it is robust and generated automatically. Properties of either the flow channel domain or yarn volume were attributed to the voxel elements. The mesh is directly exported from TexGen to ANSYS® CFX 12.0. The in-plane permeability in warp and weft direction as well as the through-thickness permeability was calculated based on Darcy's law from the average pressure drop and flow rate obtained from the CFD simulation.

5. Mechanical analysis

The composites are modelled with two constituents, the isotropic elastic matrix and the transversely isotropic resin/fibre tow. The resin system used in the composites with the orthogonal weave as reinforcement was Gurit Prime 20LV epoxy. The nominal properties of

the cured resin are listed in Table 3. The nominal carbon fibre properties are listed in the same table. The transverse modulus of carbon fibre was assumed to be 15 GPa, approximated from published experimental data [6]. These were the input constants in a hexagonally packed single fibre unit cell model. The elastic constants for the tow were derived from solving the six load cases on the unit cell in ABAQUS, shown in Figure 4. The longitudinal strength of the tow corresponds to the fracture of fibre at strain 1.8 %. The transverse tensile strength of the tow was assumed to be equal to the tensile strength of cured resin, while the longitudinal shear strength was equal to the interlaminar shear strength (Table 3). The effective tow properties are listed in Table 4.

A failure model introduced by Ruijter [7] was implemented to reduce stiffness gradually as follows:

$$E = E_0 \max(P, 0.001), \quad P = \left(1 - \frac{1}{\exp(-c_1 D + c_2)} \right) \quad (4)$$

where D is the damage parameter which is equal to ratio of stress (σ) and failure stress (F):

$$D_1 = \frac{\sigma_{11}}{F_{11}} \quad (5)$$

$$D_2 = \frac{\sqrt{\sigma_{12}^2 + \sigma_{13}^2}}{F_{12}} \quad (6)$$

$$D_3 = \left(\frac{\max(\sigma_2, \sigma_3)}{F_{22}} \right) \quad (7)$$

For damage along the fibres (Eq. 5) and transverse to the fibres (Eq. 7), the maximum stress criterion is used. For shear damage (Eq. 6), partial distortion energy is used as failure criterion.

Table 3. Nominal properties of resin matrix and fibres.

| | E (GPa) | Tensile strength (MPa) | Tensile failure strain (%) | Interlaminar shear strength (MPa) |
|-------------|---------|------------------------|----------------------------|-----------------------------------|
| Cured resin | 3.5 | 73 | 3.5 | 47 |
| Fibre | 238 | 3950 | 1.7 | - |

Table 4. Tow properties derived from FE analysis, $V_f = 70\%$.

| E_{11} (GPa) | E_{22}, E_{33} (GPa) | G_{12}, G_{13} (GPa) | G_{23} (GPa) | ν_{12}, ν_{13} | ν_{23} | Longitudinal tensile strength (MPa) | Transverse tensile strength (MPa) | Longitudinal shear strength (MPa) |
|----------------|------------------------|------------------------|----------------|----------------------|------------|-------------------------------------|-----------------------------------|-----------------------------------|
| 168.7 | 8.69 | 4.3 | 3.24 | 0.3 | 0.345 | 3036 | 69.6 | 50 |

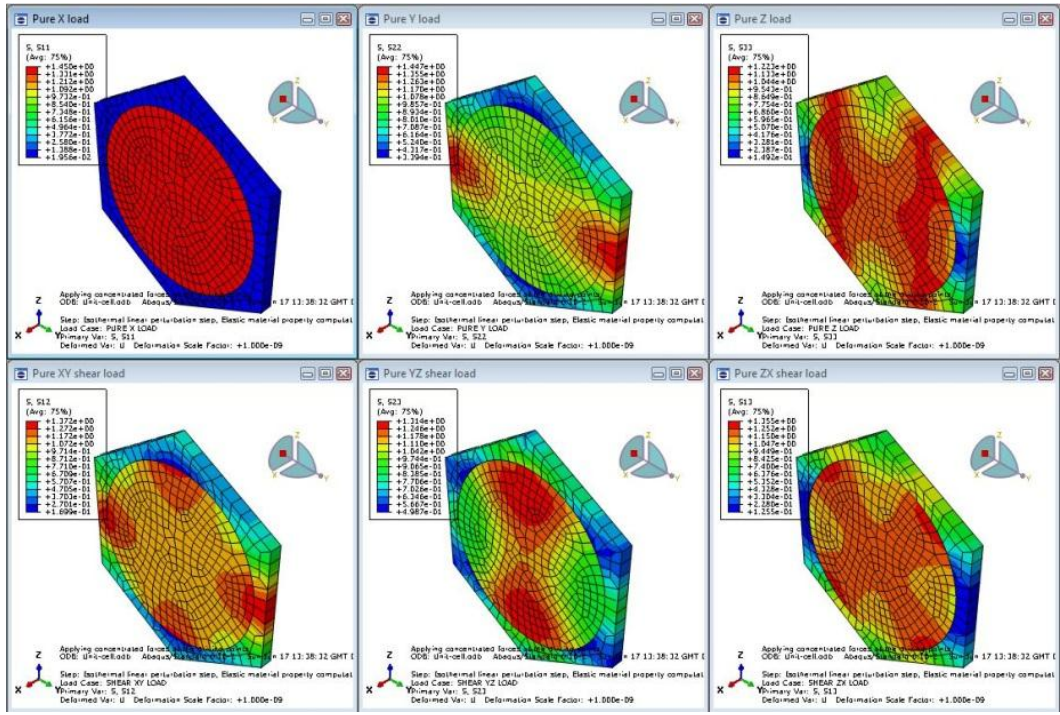


Figure 4. Screenshot of the six load cases of a single fibre unit cell model in ABAQUS for calculation of tow elastic properties.

6. Results and discussion

6.1 Permeability predictions

After assessing the sensitivity of permeability prediction on the mesh density for flow simulation, the number of elements was chosen as $50 \times 50 \times 50$ (warp \times weft \times thickness) for the unit cell mesh to obtain a reasonable balance between computation time and accuracy. To assess the sensitivity of permeability prediction on the level of detail in geometrical textile modelling, incremental variations were implemented in the geometrical models. A unit cell of the orthogonal weave was defined with average dimensions based on μ -CT image analysis (Table 2). The local refinement on binder cross-sections, surface crimp and warp yarn cross-section was made step by step in successive unit cell models. The geometrical variations addressed observations from the μ -CT images shown in Figure 5. The predictions from CFD simulations are plotted together with the experimental data in Figure 6. It demonstrates a clear benefit from local geometrical refinement for improving permeability prediction.

The same principles were applied for modelling the reinforcement with a higher fibre volume fraction, $V_f = 67\%$, under compaction. As the local geometries were well defined, the predictions are close to the experiment data (Figure 7).

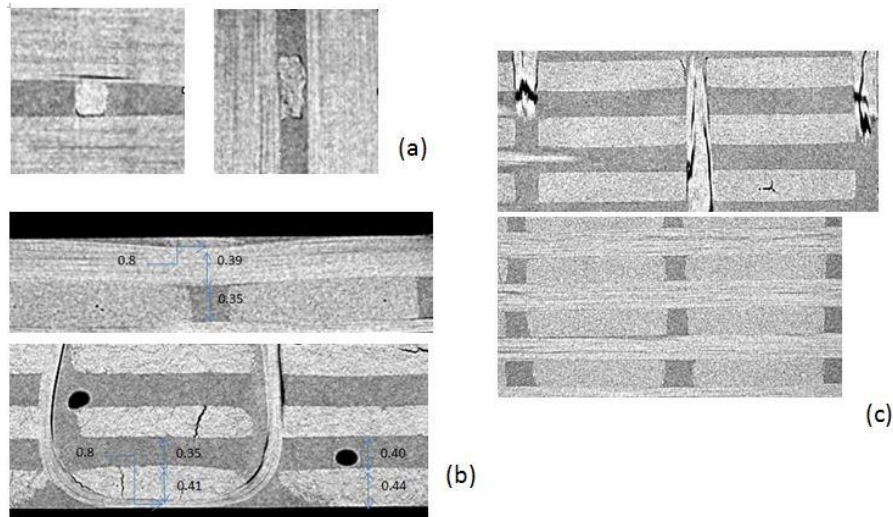


Figure 5. Local geometry variations observed in 3D μ -CT images: (a) Binder cross-sections; (b) surface yarn crimp; (c) Upper - warp cross-sections in brick shape, Lower - power elliptical weft cross-sections.

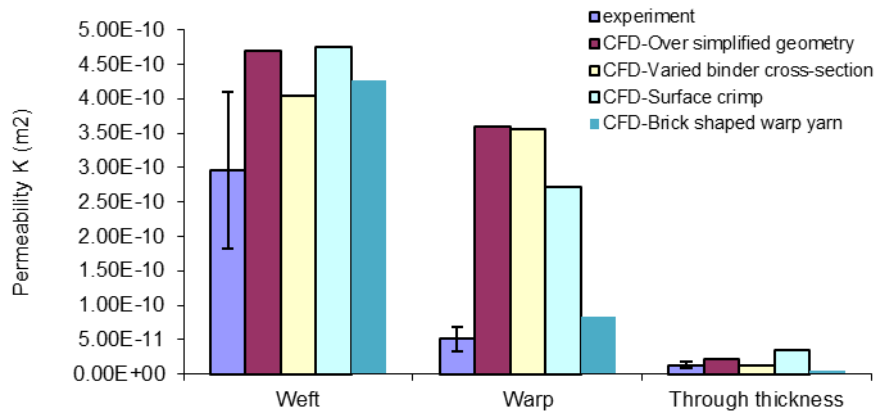


Figure 6. Permeability predictions with incremental local geometry variations, $V_f = 55\%$.

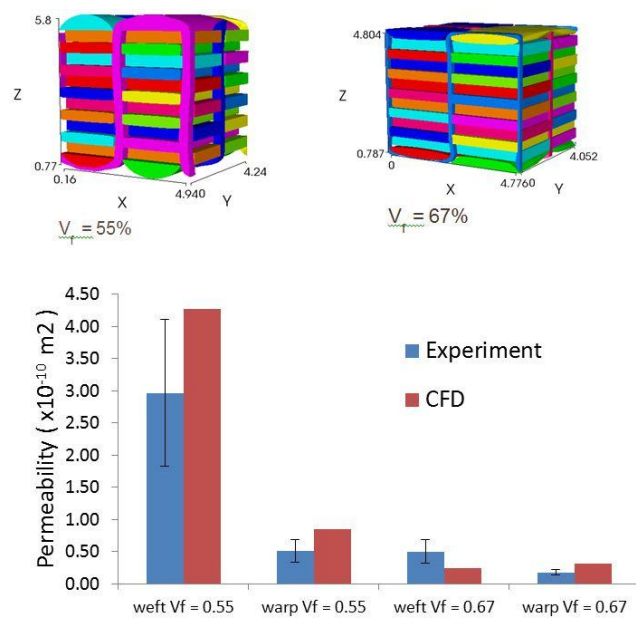


Figure 7. Permeability predictions for the orthogonal weave at two compaction levels, corresponding to $V_f = 55\%$ and $V_f = 67\%$.

6.2 Strength predictions

To predict the mechanical properties of composites with the orthogonal weave as reinforcement (at $V_f = 55\%$), loading of the unit cell beyond fracture up to a strain of 2 % was simulated by setting appropriate periodic boundary conditions in warp and weft direction and free boundary for top and bottom surfaces. The weave construction of the orthogonal fabric contains 7 plies in weft direction and 6 plies in warp as described in Table 1. Theoretically, if all tows are perfectly straight, as weft to warp ply ratio is 7/6, the stiffness in weft direction would be 17 % higher than in warp direction if the contribution by the binder is neglected. In fact, because the unit cell model describes surface crimp in weft yarns as representing the actual geometry, stiffness in weft is lower. Plotted in Figure 8 are the stress versus strain curves, showing that the stiffness values are close in warp and weft directions. The ultimate strength, however, is different in warp and weft directions. The failure was initiated at a much earlier stage while loading in weft direction. The fracture occurs near the crossover with the binder yarn. Two mechanisms are involved: firstly surface crimp at the crossover points introduces local stress concentrations; secondly reaction force from binder through straightening crimp in the weft direction accelerates transverse failure via resin cracking (Eq. 5), illustrated in Figure 9. The fibre fracture starts to manifest after sufficient resin cracks accumulate on plane of the binder path. It leads to much lower strength in the crimped weft direction than the warp. The unit cell with the local geometry refinement captures this effect well.

A detailed experimental study for validation is currently underway.

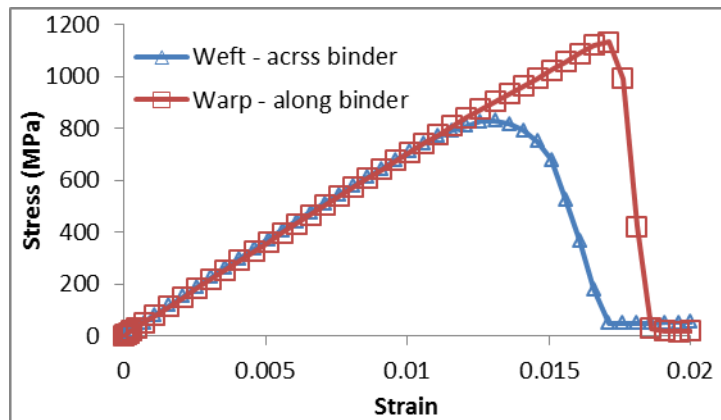


Figure 8. FE prediction of tensile response of the orthogonal reinforced composites, $V_f=55\%$.

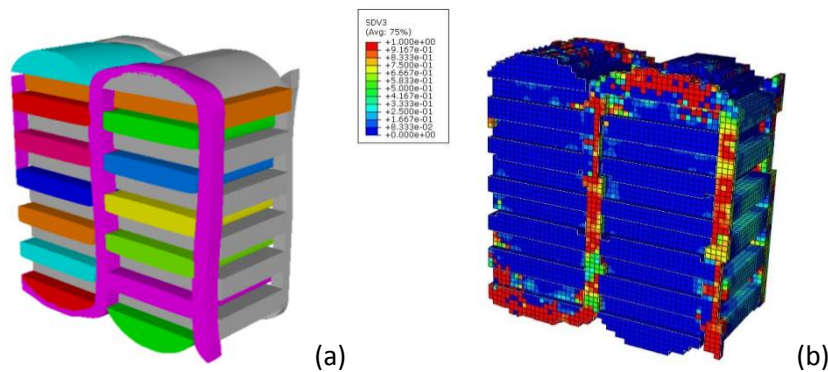


Figure 9. Failure initiation and propagation in plane of binder path under tensile loading in weft direction across binder path.

7. Conclusions

A systematic approach was presented to assess the effect of local geometrical variations on composites processing and mechanical properties. The motivation was to highlight the geometrical features essential for accurate modelling of 3D woven composites and quantify the relationship between geometry and performance. For the example of a 3D orthogonal weave reinforcement, the geometry of the composites was characterised in detail by μ -CT image analysis. The geometrical models were generated in TexGen in a semi-automated manner with local geometrical refinements. Based on these models, CFD simulation of impregnating flow and static mechanical analysis were carried out for prediction of in-plane permeability and in-plane tensile properties, respectively. With inclusion of local variations in geometrical modelling, the predictions of permeability improved significantly compared with the experimental data. The prediction of mechanical strength also revealed different failure mechanisms in warp and weft directions, as there are local geometrical differences in crimp, binder configuration and yarn cross-sectional shapes.

Acknowledgements

This work was supported by the Engineering and Physical Sciences Research Council [grant number: EP/IO33513/1], through the EPSRC Centre for Innovative Manufacturing in Composites.

References

1. Mouritz, A.P., Three-dimensional (3D) fibre reinforcements for composites, in Boisse, P. (Ed.), *Composite reinforcements for optimum performance*, Woodhead Publishing, UK, 2011
2. Long, A.C. and Brown, L.P., Modelling the geometry of textile reinforcements for composites: TexGen, in Boisse, P. (Ed.), *Composite reinforcements for optimum performance*, Woodhead Publishing, UK, 2011
3. Weisstein, E.W., Superellipse, From *MathWorld--A Wolfram Web Resource*. <http://mathworld.wolfram.com/Superellipse.html>
4. Gebart, B.R., Permeability of Unidirectional Reinforcements for RTM, *Journal of Composite Materials*, **26**(8), 1100-1133, 1992
5. Endruweit, A., McGregor, P., Long, A.C. and Johnson, M.S., Influence of the fabric architecture on the variations in experimentally determined in-plane permeability values, *Composites Science and Technology*, **66**(11-12), 1778-1792, 2006
6. Maurin, R., Davies, P., Baral, N. and Baley, C., Transverse Properties of Carbon Fibres by Nano-Indentation and Micro-mechanics, *Applied Composite Materials*, **15**(2), 61-73, 2008
7. Ruijter, W., Analysis of mechanical properties of woven textile composite as functions of textile geometry, PhD dissertation, School of M3, University of Nottingham, Nottingham, UK, 2008